УДК 539.3

MODELLING SHOCK WAVES IN COMPOSITE MATERIALS

© 2010 A.A. Lukyanov[1]

An accurate extrapolation of high-pressure shock Hugoniot states to other thermodynamics states for shocked Carbon Fibre Composite (CFC) materials is presented. The proposed anisotropic equation of state represents mathematical and physical generalization of the Mie-Grüneisen equation of state for isotropic material and reduces to this equation in the limit of isotropy. Using an anisotropic nonlinear continuum framework and generalized decomposition of a stress tensor, the shock waves propagation in CFC materials is examined. A numerical calculation showed that Hugoniot Stress Levels (HELs) agree with the experimental data for selected CFC material. The results are presented and discussed, and future studies are outlined.

Key words: composite structures, shock wave, modelling, stress decomposition, equation of state, impact.

Introduction

Investigation of anisotropic composite materials (e.g., CFC materials) behavior has found significant interest in the research community due to the widespread application of anisotropic composite materials in aerospace and civil engineering problems. For example, composite materials are one of the main materials in the construction of modern aircraft. The dynamic mechanical behavior of anisotropic composite materials in air vehicles is important for applications involving impact and dynamic loading. These applications cover a wide range of situations such as crashworthiness and protective armors in air and space vehicles and other applications. Since shock wave phenomenon is involved in many physical phenomena, we are interested in understanding the composite material mechanical properties under these non-trivial conditions (i.e., shock loading conditions).

[1]Lukyanov Alexander Alekseevich (aaluk@mail.ru), Abingdon Technology Centre, Research & Development, Schlumberger, Abingdon OX14 1UJ, United Kingdom, Lipetsk, 398059, Russia.

Modern, high-resolution methods to monitoring the stress and particle velocity histories in shock waves and equipment have been created (e.g. Barker and Hollenbach [1]; Kanel [2]; Kanel *et al.* [3]; Bourne and Stevens [4]; Bourne [5]). A common technique for the study of material behaviour under shock loading is the planar plate impact test (one-dimensional shock wave propagation). This method impacts an accurately machined flyer plate onto an equally accurately machined target plate that has been instrumented such that useful data can be obtained. In most cases, the loading axis has been normal to the plane of the fibres (i.e. the through thickness orientation). Shock wave experiment has frequently provided the motivation for the construction of material constitutive relations and has been the principal means for determining material parameters for some of these relations (Davison and Graham [6]; Steinberg [9]; Bushman *et al.* [7]; Meyers [9]). For example, Dandekar *et al.* [10] investigated the equation of state of a glass fibre–epoxy composite, in terms of the shock stress, shock velocity U_s and particle velocity u_p (i.e. the velocity of material flow behind the shock front). Their results indicated that there was a linear relationship between shock and particle velocity. This type of behavior is typical of a wide range of materials, including metals (Steinberg [9]; Meyers [9])) and some polymers, including epoxy resins (Munson and May [11]; Millett *et al.* [12]) and composite (Zhuk *et al.* [13]), including carbon fibre–epoxy composite (Riedel *et al.* [14]) and glass fibre–epoxy composite (Zaretsky *et al.* [15]). A linear U_s–u_p relationship shows that in the through thickness orientation, this class of composite displays fairly typical experimental data. However, in spite of a perfectly adequate general understanding, experimental methodology, and theory, material models do not agree in detail, especially for anisotropic composite materials.

The purpose of this paper is the numerical investigation of the shock wave propagation in composite materials, and more specifically, for anisotropic Carbon Fibre Composite (CFC) materials. A fiber-reinforced composite is heterogeneous by definition (e.g., Kanel *et al.* [16]), composed of two main constituents, i.e. a mixture of stiff fibres (usually glass or carbon although sometimes Kevlar is used) in a polymeric binder (most often epoxy). These fibres can be unidirectional, or in two- or three-dimensional weaves. For many years, it has been assumed that the response of composite materials to shock loading is isotropic (e.g., Chen *et al.* [17]; Hayhurst *et al.* [18]), and only recently has anisotropy in the shock response of composite materials attracted the attention of researchers (e.g., Bordzilovsky *et al.* [19]; Hereil *et al.* [20]; Millett *et al.* [21]). Modern hydrocode shock modelling capabilities are confined almost exclusively to isotropic media; little provision has been made for anisotropic materials. Several different approaches can be adopted. In this paper, we have chosen to work in a macroscopic continuum, and modify existing computational tools formulated for isotropic continuum (Kiselev and Lukyanov [22]). The composite materials response under shock loading leads to a nonlinear behavior (i.e., large compressions), therefore, an equation of state (EOS) is required (e.g. Anderson *et al.* [23]; Lukyanov [24, 25, 26]; Lukyanov and Pen'kov [28]). To address this issue, thermodynamically consistent framework for modelling the response of composite materials under shock loading was developed. This framework, building on the thermodynamic approach of Wallace [30] and continuum framework of Johnson [31, 32], using nonlinear elasticity within a thermodynamically consistent numerical incremental formalism (e.g., Winey and Gupta [33]).

1. An anisotropic equation of state (EOS)

The definition of pressure in the case of an anisotropic solids should be the result of stating that the "pressure" term should only produce a change of scale, i.e. isotropic state of strain. The generalized decomposition of the stress tensor σ_{ij} is defined as (Lukyanov [24, 25, 26, 27]; Lukyanov and Pen'kov [28, 29]):

$$\sigma_{ij} = -p^* \alpha_{ij} + \tilde{S}_{ij}, \quad \alpha_{ij}\tilde{S}_{ij} = 0, \quad \tilde{S}_{ij} = \sigma_{ij} - \alpha_{ij}\frac{\sigma_{kl}\alpha_{kl}}{\alpha_{kl}\alpha_{kl}}, \tag{1.1}$$

where $p^*\alpha_{ij}$ is the generalized spherical part of the stress tensor, $\tilde{S}_{ij}$ is the generalized deviatoric stress tensor, p^* is the total generalized "pressure" and α_{ij} is the first generalization of the Kronecker's delta symbol. The summation convention is implied by the repeated indices. The procedure of construction for the tensor α_{kl} has been defined by Lukyanov [24, 25, 26, 27]. The elements of the tensor α_{kl} are

$$\begin{gathered}\alpha_{11} = \left(\sum_{k=1}^{3} C_{k1}\right) 3\bar{K}_C, \ \ \alpha_{22} = \left(\sum_{k=1}^{3} C_{k2}\right) 3\bar{K}_C, \\ \alpha_{33} = \left(\sum_{k=1}^{3} C_{k3}\right) 3\bar{K}_C, \ \ \alpha_{ij}\alpha_{ij} = 3,\end{gathered} \tag{1.2}$$

$$\begin{gathered}K_C = \frac{1}{3\sqrt{3}}\sqrt{\left(\sum_{k=1}^{3} C_{k1}\right)^2 + \left(\sum_{k=1}^{3} C_{k2}\right)^2 + \left(\sum_{k=1}^{3} C_{k3}\right)^2}, \\ K_C = \frac{1}{9\bar{K}_C},\end{gathered} \tag{1.3}$$

where C_{ij} is the elastic stiffness matrix (written in Voigt notation).

For anisotropic materials (e.g., composite materials) under shock loading, the total generalized "pressure" p^* has been expressed [25, 26], [28] as:

$$p^* = p^{EOS} + \frac{\beta_{ij}\tilde{S}_{ij}}{\beta_{kl}\alpha_{kl}}, \tag{1.4}$$

where p^{EOS} is the pressure related to an equation of state and β_{ij} is the second generalization of the Kronecker's delta symbol (Lukyanov [24, 25, 26, 27]). The extrapolation has been done by using a very popular form of equation of state

p^{EOS} that is used extensively for isotropic solid continua is the Mie-Grüneisen EOS:

$$p^{EOS} = f(\rho, e) = P_H \cdot \left(1 - \frac{\Gamma(\nu)}{2}\mu\right) + \rho\Gamma(\nu)e, \ \ \nu = \frac{1}{\rho}, \tag{1.5}$$

$$U = c + S_1 u_p + S_2 \left(\frac{u_p}{U}\right) u_p + S_3 \left(\frac{u_p}{U}\right)^2 u_p, \tag{1.6}$$

or

$$p^{EOS} = \begin{cases} \dfrac{\rho_0 c^2 \mu \left[1 + \left(1 - \frac{\Gamma}{2}\right)\mu - \frac{\Gamma}{2}\mu^2\right]}{\left[1 - (S_1 - 1)\mu - S_2 \frac{\mu^2}{\mu+1} - S_3 \frac{\mu^3}{(\mu+1)^2}\right]^2} + \\ \quad + (1+\mu)\cdot\Gamma\cdot E, \quad \mu > 0; \\ \rho_0 c^2 \mu + (1+\mu)\cdot\Gamma\cdot E, \quad \mu < 0; \end{cases} \tag{1.7}$$

$$c \in \left[\sqrt{\frac{K_S}{\rho_0}}, \sqrt{\frac{K_C}{\rho_0}}\right], \ \ \nu = \frac{1}{\rho}, \ \ E = \frac{e}{\rho_0}, \tag{1.8}$$

where P_H is the Hugoniot pressure, e is the specific internal energy, E is the internal energy per initial density, μ is the relative change of volume, ρ is the density, $\Gamma(\nu)$ is the Grüneisen's gamma, ν is the specific volume, S_1, S_2, S_3 are the intercept of the U-u_p cubic curve [9], U is the shock velocity, u_p is the particle velocity directly behind the shock. Parameters $c \in [c_{II}, c_I]$, S_1, S_2, S_3, γ_0, a represent material properties which define its EOS (1.7). Note that the generalized decomposition of the stress tensor can be applied for all composite materials of any symmetry and represents a mathematically consistent generalization of the conventional isotropic case. The elements of the tensor β_{kl} are

$$\begin{gathered} \beta_{11} = \left(\sum_{k=1}^{3} J_{k1}\right) 3K_S, \ \ \beta_{22} = \left(\sum_{k=1}^{3} J_{k2}\right) 3K_S, \\ \beta_{33} = \left(\sum_{k=1}^{3} J_{k3}\right) 3K_S, \ \ \beta_{ij}\beta_{ij} = 3, \end{gathered} \tag{1.9}$$

$$\frac{1}{K_S} = \sqrt{3}\sqrt{\left(\sum_{k=1}^{3} J_{k1}\right)^2 + \left(\sum_{k=1}^{3} J_{k2}\right)^2 + \left(\sum_{k=1}^{3} J_{k3}\right)^2}, \tag{1.10}$$

where J_{ij} are elements of compliance matrix (written in Voigt notation), K_S represents the second generalized bulk modulus. In the limit of isotropy, the proposed generalization returns to the traditional classical case where tensors α_{ij}, β_{ij} equal δ_{ij} and parameters K_C and K_S reduce to the well-know expression for conventional isotropic bulk modulus. This completes the derivation of the generalized decomposition of the stress tensor for anisotropic materials.

The geometrical representation of generalized decomposition of the stress can be shown in the principal stress space (Haigh-Westergaard stress space) for α-decomposition of the stress tensor and β-decomposition of the stress tensor in the principal strain space. Figure 1.1 shows schematic representation of α-decomposition of the stress tensor, where α-direction is described by the tensor α_{ij} and δ-direction is described by the Kronecker's delta tensor δ_{ij}. Therefore, p_δ describes the hydrostatic stress (isotropic stress), $p^* \neq p_\delta$ describes the total generalized hydrostatic stress (or anisotropic total generalized hydrostatic stress), and $p \neq p^* \neq p_\delta$ is the generalized pressure related to an equation of state (EOS). The angle between α-direction and δ-direction is described by the variable ψ which can be obtained from $\cos\psi = \frac{\alpha_{11}+\alpha_{22}+\alpha_{33}}{3}$. Similar representation can be shown for β-decomposition of the stress tensor.

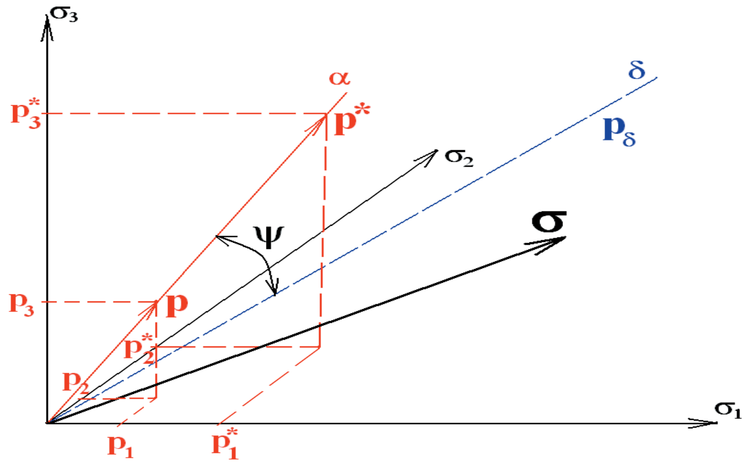

Fig. 1.1. Schematic representation of α-decomposition of the stress tensor

2. Shock wave propagation in CFC materials

The plane shock-wave technique provides a powerful tool for studying different material properties [7]–[16], [17]–[22], [25, 26] and assessing a proposed theoretical model by comparing its predictions with experimental data. From an experimental point of view, it is clear that the generation of shock waves in a composite target and the measurement of their characteristics, such as speed and intensity, provide one of the most convenient methods of investigating the physical properties of a composite material under high pressures. The theoretical prediction of features of wave propagation in specified loading conditions can provide simple basic test for assessment of a proposed theoretical model by comparing its predictions with experimental data. In this section, plane wave numerical experiments will be used to determine the Hugoniot Stress Limit (HEL) (i.e. stress level associated with the shock wave) and the dynamic compressibility for selected anisotropic carbon-fibre composite (CFC).

2.1. Description of Experiment

The work discussed below concerns the shock response of a carbon-fibre / epoxy composite. This is done by the technique of plate impact, whereby a flat plate of constant thickness and a known material (for instance aluminium alloy, or copper) is impacted onto a target plate made from the test material. The flyer plates are launched using a 50 mm bore, 5 m long single stage gas gun. On impact, a planar shock front starts propagating into the target. The shock propagation in the target is monitored using manganin stress gauges, placed at different locations within the target assembly.

The plate impact test was done at Defence Academy of the United Kingdom by Millett *et al.* [21] using samples of a carbon-fibre composite (CFC) of thicknesses 3.8 mm thick. A manganin stress gauge was supported on the back of the specimen plate with a 12 mm block of polymethylmethacrylate (PMMA). Also, the gauge was also backed into the PMMA by approximately 1.5 mm PMMA offset block to act as extra protection for the gauge. A second gauge (the 0 mm position) was supported on the front of the target assembly with a 1 mm plate of aluminium alloy 6082-T6. Shock stresses were induced with dural flyer plates impacted with the velocity 504 m/s, using a single stage gas gun the Defence Academy of the United Kingdom [21]. The impact axis was normal to the plane of the fibres. A schematic of the target assembly and gauge placement is shown in Figure 2.1. The results from the stress gauges

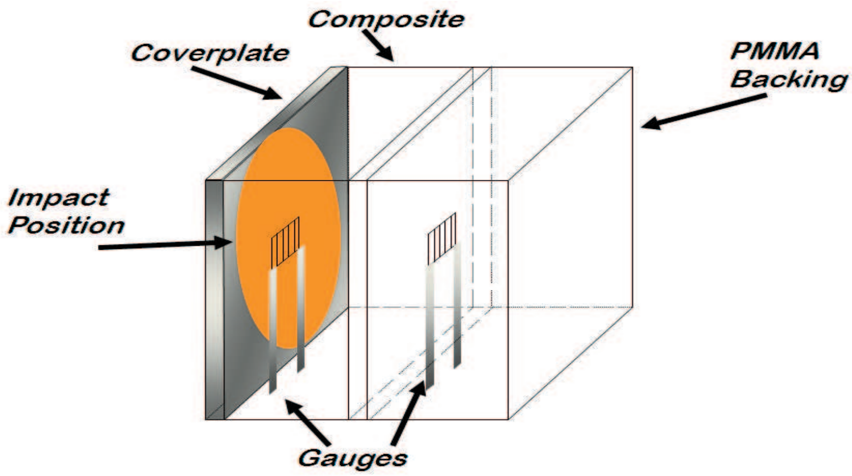

Fig. 2.1. Schematic diagram of the experimental target assembly

were converted to in material (Target) values σ_M, using the shock impedances of the target A_T and PMMA A_P, via the well-known relation:

$$\sigma_M = \frac{A_T + A_P}{2A_P}\sigma_P, \tag{2.1}$$

where σ_P is the stress gauges values. The equivalent material properties of the CFC composite plate were chosen to match the layer macromechanical properties for the layup $[0/90, \pm 45]_4$ and the longitudinal sound speed in the through-thickness orientation [21]. Material properties of CFC material (z — direction corresponds to the through the thickness direction, x — direction corresponds to the fill direction, and y — direction to the wrap direction) are $\rho_0 = 1500\ kg/m^3$, $E_x = 68,467\ GPa$, $E_y = 66,537\ GPa$, $E_z = 13,678\ GPa$, $\nu_{yx} = 0,04$, $\nu_{zx} = 0,0045$, $\nu_{zy} = 0,0044$, $\alpha_{11} = 1,2290$, $\beta_{11} = 0,3155$, $\alpha_{22} = 1,1956$, $\beta_{22} = 0,3254$ and $\alpha_{33} = 0,2454$, $\beta_{33} = 1,6717$.

2.2. Mathematical Framework

Plate-impact numerical simulations were performed by solving conventional conservation laws (dealing with mass, linear momentum and internal energy) for monopolar media in Cartesian coordinate system $Oxyz$ (the z — axis is perpendicular to the plate surface). In this paper, the case is considered where the diameters of the flyer and the target are much greater than their thicknesses and the characteristic time of the process is the time of several runs of elastic waves across the thickness of the target plate. In such a case, the problem may be solved using a uniaxial strain state (one-dimensional mathematical formulation in strain space) and the adiabatic approximation; therefore, the equations for planar one-dimensional shock waves can be written as:

$$\frac{1}{\rho}\frac{d\rho}{dt} = -\dot{\varepsilon}, \quad \rho\frac{dv}{dt} = \frac{\partial\left(-p^*\alpha + \tilde{S}\right)}{\partial z}, \quad \rho\frac{de}{dt} = \left(-p^*\alpha + \tilde{S}\right)\dot{\varepsilon}. \tag{2.2}$$

Here $v = v_z = v_3$ is the velocity, $\dot{\varepsilon} = \dot{\varepsilon}_{zz} = \dot{\varepsilon}_{33} = \dfrac{\partial v}{\partial z}$ is the strain rate, $\alpha = \alpha_{zz} = \alpha_{33}$, $\tilde{S} = \tilde{S}_{zz} = \tilde{S}_{33}$, $\dfrac{d}{dt}$ is the substantial derivative with respect to time. These aforementioned equations (2.2) are coupled with the appropriate constitutive equations (1.1)–(1.10). A second order in time and space $\bar{O}(\Delta t^2, \Delta z^2)$ finite difference method was employed to solve the resulting system (2.2) [22]:

$$\begin{gathered}
\frac{1}{\rho^{n+1/2}}\left[\frac{\rho^{n+1}-\rho^n}{\Delta t^{n+1/2}}\right] = -\dot{\varepsilon}^{n+1/2}, \\
\rho^{n+1/2}\left[\frac{v^{n+1}-v^n}{\Delta t^{n+1/2}}\right] = \frac{\partial\left(-p^*\alpha + \tilde{S}\right)^n}{\partial x^n}, \\
\rho^{n+1/2}\left[\frac{e^{n+1}-e^n}{\Delta t^{n+1/2}}\right] = \left(-p^*\alpha + \tilde{S}\right)^{n+1/2}\dot{\varepsilon}^{n+1/2}, \\
x^{n+1} = x^n + v^{n+1/2}\Delta t^{n+1/2}.
\end{gathered} \tag{2.3}$$

Note that a second order finite difference scheme in space was implicitly applied in system (2.3). The constitutive equations are implemented using a conventional time-centering method:

$$\bar{\sigma}_{ij}^{n+1} = \sigma_{ij}^{n} + \left[\sigma_{ik}^{n}\omega_{jk}^{n+1/2} + \omega_{ik}^{n+1/2}\sigma_{kj}^{n} + \left(\sigma^{\nabla}\right)_{ij}^{n+1/2}\right]\Delta t^{n+1/2}, \tag{2.4}$$

$$\left(\sigma^{\nabla}\right)_{ij}^{n+1/2} = \mathbf{C}_{ijkl}\dot{\varepsilon}_{kl}^{n+1/2}, \Delta\varepsilon_{kl}^{n+1/2} = \dot{\varepsilon}_{kl}^{n+1/2}\Delta t^{n+1/2}, \tag{2.5}$$

where $\bar{\sigma}_{ij}^{n+1}$ is the trial stress tensor at time t^{n+1} (calculated using elasticity constitutive equations), σ_{ij}^{n} is the true stress tensor at time t^{n}, $\omega_{jk}^{n+1/2}$ is the spin tensor (skew-symmetric part of the velocity gradient) at time $t^{n+1/2}$ (for uniaxial strain state: $\omega_{jk}^{n+1/2} = 0$), $\dot{\varepsilon}_{kl}^{n+1/2}$ is the strain rate (symmetric part of the velocity gradient) at time $t^{n+1/2}$ (for uniaxial strain state: $\dot{\varepsilon}_{kl}^{n+1/2} \neq 0$, $k, l = 1$ only), ∇ denotes a Jaumann stress rate tensor at time $t^{n+1/2}$, $\mathbf{C}_{ijkl}$ is the elastic stiffness matrix, and $\Delta t^{n+1/2}$ is the time step. During the constitutive model calculations, the stresses and state variables are known at the start of each increment and their values are updated at the end of the increment, according to the change in total strain increment. Using relations (2.4), (2.5) and the generalized decomposition of the stress tensor specified by equations (1.1)–(1.10), the expression for true generalized deviatoric stress tensor and stress tensor can be written in the form:

$$\tilde{S}_{ij}^{n+1} = \bar{\sigma}_{ij}^{n+1} - \alpha_{ij}\frac{\bar{\sigma}_{ij}^{n+1}\alpha_{kl}}{\alpha_{kl}\alpha_{kl}}, \quad \sigma_{ij}^{n+1} = -\alpha_{ij}\left(p^{*}\right)^{n+1} + \tilde{S}_{ij}^{n+1}, \tag{2.6}$$

where $\tilde{S}_{ij}^{n+1}$ is the true generalized deviatoric stress tensor at time t^{n+1}, σ_{ij}^{n+1} is the true stress tensor at time t^{n+1}, $\left(p^{*}\right)^{n+1}$ is the true total generalized pressure, α_{ij} is the first generalized Kronecker symbol. Note that the equation of state (1.5) is linear in internal energy, e, meanwhile the equation for the specific internal energy (2.2) is linear in p^{*}. Therefore, the algorithm for true generalized pressure $\left(p^{*}\right)^{n+1}$ and specific internal energy e^{n+1} comprises the following system of equations:

$$\begin{gathered}\left(p^{EOS}\right)^{n+1} = P_{H}^{n+1}\cdot\left(1 - \frac{\Gamma^{n+1}}{2}\mu^{n+1}\right) + \\ +\rho^{n+1}\Gamma^{n+1}e^{n+1} = A^{n+1} + B^{n+1}e^{n+1},\end{gathered} \tag{2.7}$$

$$e^{n+1} = \tilde{e}^{n+1} - \frac{1}{2}\nu^{n+1/2}\varepsilon_{\alpha}^{n+1/2}\Delta t^{n+1/2}\left(p^{EOS}\right)^{n+1}, \tag{2.8}$$

$$\begin{gathered}\tilde{e}^{n+1} = e^{n} + \nu^{n+1/2}\tilde{S}^{n+1/2}\dot{\varepsilon}^{n+1/2}\Delta t^{n+1/2} - \\ -\frac{1}{2}\nu^{n+1/2}\left[\left(p^{*}\right)^{n} + \frac{\beta_{ij}\tilde{S}_{ij}^{n+1}}{\beta_{kl}\alpha_{kl}}\right]\dot{\varepsilon}_{\alpha}^{n+1/2}\Delta t^{n+1/2} - \\ -\nu^{n+1/2}Q^{n+1/2}\dot{\varepsilon}_{\delta}^{n+1/2}\Delta t^{n+1/2},\end{gathered} \tag{2.9}$$

$$\dot{\varepsilon}_{\alpha}^{n+1/2} = \dot{\varepsilon}_{xx}^{n+1/2}\alpha_{xx}, \quad \dot{\varepsilon}_{\delta}^{n+1/2} = \dot{\varepsilon}_{xx}^{n+1/2}\delta_{xx}, \tag{2.10}$$

$$\nu^{n+1/2} = \frac{1}{2}\left(\nu^{n+1} + \nu^{n}\right), \quad \left(p^{*}\right)^{n+1/2} = \frac{1}{2}\left[\left(p^{*}\right)^{n+1} + \left(p^{*}\right)^{n}\right]. \tag{2.11}$$

Thus, equation (2.7)–(2.8) can be written in the form [34]:

$$\left(p^{EOS}\right)^{n+1} = \frac{A^{n+1} + B^{n+1}\tilde{e}^{n+1}}{1 + \frac{1}{2}B^{n+1}\nu^{n+1/2}\dot{\varepsilon}_{\alpha}^{n+1/2}\Delta t^{n+1/2}},$$
$$e^{n+1} = \tilde{e}^{n+1} - \frac{1}{2}\nu^{n+1/2}\varepsilon_{\alpha}^{n+1/2}\Delta t^{n+1/2}\left(p^{EOS}\right)^{n+1}, \qquad (2.12)$$

where $\left(p^{EOS}\right)^{n+1}$ is the true equation of state pressure at time t^{n+1}, $Q^{n+1/2}$ is the artificial bulk viscosity at time $t^{n+1/2}$, ν^{n+1} is the specific volume at time t^{n+1}, P_H^{n+1} is the Hugoniot pressure at time t^{n+1}, μ^{n+1} is the relative change of volume at time t^{n+1}, ρ^{n+1} is the density at time t^{n+1}, Γ^{n+1} is the Grüneisen's gamma at time t^{n+1}, β_{ij} is the second generalized Kronecker symbol.

2.3. Modelling Shock Waves in CFC Materials

In this section, the shock wave propagation within composite material is considered. Although, a flyer plate and supporting plate at the front of the target assembly (the 0 *mm* position, see Fig. 2.1 were made using Al 6082-T6, the well-tabulated material properties of Al 6061-T6 were used during numerical simulations for Al 6082-T6. The aluminium 6061-T6 was modelled using well-established Prandtl-Reuss elastic-plastic model combined with well-tabulated Steinberg-Guinan's yield strength model [9] and EOS (1.7):

$$2G\dot{e}_{ij} = S_{ij}^{\nabla} + \lambda S_{ij}, \;\; \dot{e}_{ij} = \dot{\varepsilon}_{ij} - \frac{\dot{\varepsilon}_{kk}}{3}\delta_{ij}, \;\; S_{ij} = \sigma_{ij} - \frac{\sigma_{kk}}{3}\delta_{ij},$$
$$S_{ij}S_{ij} \leqslant \frac{2}{3}Y^2, \;\; \lambda = \left[\frac{3\dot{e}_{ij}S_{ij} - YY^{\nabla}}{Y^2}\right] H\left(S_{ij}S_{ij} - \frac{2}{3}Y^2\right), \qquad (2.13)$$

$$Y = Y_0 \cdot \left(1 + \beta\varepsilon_{ef}^{p}\right)^n \left[1 + bp^{EOS}\left(\frac{\rho_0}{\rho}\right)^{1/3} - h(T - T_0)\right],$$
$$Y_0\left(1 + \beta\varepsilon_{ef}^{p}\right)^n \leqslant Y_{max}, \;\; Y = 0 \quad \text{if} \quad T \geqslant T_m \;,$$
$$T_m = T_{m0}\left(\frac{\rho_0}{\rho}\right)^{-2(\gamma_0 - a - 1/3)} \cdot \exp\left[2a\left(1 - \frac{\rho_0}{\rho}\right)\right], \qquad (2.14)$$
$$G = G_0\left[1 + bp^{EOS}\left(\frac{\rho_0}{\rho}\right)^{1/3} - h(T - T_0)\right],$$

where $\dot{e}_{ij}$ is the strain rate deviator, S_{ij} is the stress deviator, p^{EOS} is the EOS pressure (1.7), Y is the yield strength, Y_0 is the yield strength at the Hugoniot Elastic Limit (HEL), Y_{max} is the work-hardening maximum, ε_{ef}^{p} is the effective plastic strain, β, n are work-hardening parameters, T_{m0} is the melt temperature at constant volume, h is the temperature dependence of the shear modulus, b is the pressure dependence of the shear modulus, $H(\cdot)$ is the Heviside function. In this paper, the isothermal approximation is considered for all materials, i.e. $T = T_0$. Material properties used for the aluminium alloy (Al 6061-T6) are:

density, $\rho_0 = 2703\ kg/m^3$; shear modulus, $G_0 = 27,6\ GPa$; yield strength, $Y_0 = = 290\ MPa$; pressure dependence of the shear modulus, $b = 6,52 \cdot 10^{-2}\ GPa^{-1}$; work-hardening parameters, $\beta = 125$ and $n = 0,10$; maximum yield strength, $Y_{max} = 680\ MPa$ [9]. The parameters of the Mie-Grüneisen EOS (1.7) for Al 6061-T6 are: $c = 5240\ m/s$, $S_1 = 1,4$, $S_2 = 0$, $S_3 = 0$, $\gamma_0 = 1,97$ and $a = 0,48$ [9].

Based on the characteristics of this plate impact problem, the plates (numerical domains), which are used in the numerical simulation, are modelled as 1D bars [22]. The 1D mesh resolutions were sufficient to allow the resolution of all the relevant waves in the target and flyer. The stress time histories were recorded at the 0 mm position of the target plate (the first Finite Difference (FD) element in the target plate (CFC) connected to cover plate) and at the back of the test specimen (the first Finite Difference (FD) element in the PMMA connected to PMMA offset block). Stress in the z − direction at the front surface of the CFC materials is compared to the measurements from the rear gauge. During the through-thickness test and simulation, the shock front is planar and parallel to the composite plies. Consequently the stress measured by the gauge and the stress in the corresponding FD elements are directly comparable. The plate impact test used for model validation was performed with the impact velocity of 504 m/s and with a 3.8 mm thick composite target plate, 5 mm thick aluminium alloy flyer plate. The front gauge was covered with a 1 mm aluminium alloy plate while the back gauge was backed with 12 mm of PMMA block and $1,5$ mm PMMA offset block. Therefore, the PMMA material was also modelled in the present work using well-established Prandtl-Reuss elastic-plastic model combined with Steinberg-Guinan's yield strength model. Material properties and EOS data for the PMMA, used in the numerical simulation, are: initial density $\rho_0 = 1182\ kg/m^3$; shear modulus, $G_0 = 23,2\ GPa$; yield strength, $Y_0 = 65\ MPa$; pressure dependence of the shear modulus, $b = 0,2\ GPa^{-1}$; work-hardening parameter, $n = 0.1$; maximum yield strength, $Y_{max} = 420\ MPa$ and, partially, were taken from [9]. The parameters of the Mie-Grüneisen EOS (1.7) for PMMA are: $c = = 2180\ m/s$, $S_1 = 2,088$, $S_2 = -1,124$, $S_3 = 0$, $\gamma_0 = 0,85$ and $a = 0,0$.

Assessing a proposed theoretical model Eqs. (1.1)–(1.10) by comparing its predictions (using different EOS data) with experimental data, the optimal EOS data for CFC composite material are defined as $c = 3590\ m/s$, $S_1 = = 10,755$, $S_2 = 0$, $S_3 = 0$, $\gamma_0 = 0,85$ and $a = 0,50$. Figure 2.2 shows the final comparison between experimental data and the numerical simulation resulting from the new anisotropic equation of state and specified EOS data. The stress in the z-direction at the front surface of the composite material is compared to the stress history from the front gauge Fig. 2.1, while the stress in PMMA is compared to the measurements from the rear gauge Fig. 2.1. The comparison shows that the maximum stress pulse width is approximately $2,067\ \mu s$ (numerical simulation) and $2,122\ \mu s$ (experimental data) at the front surface of the composite material (see Fig. 2.2), and approximately $2,36\ \mu s$

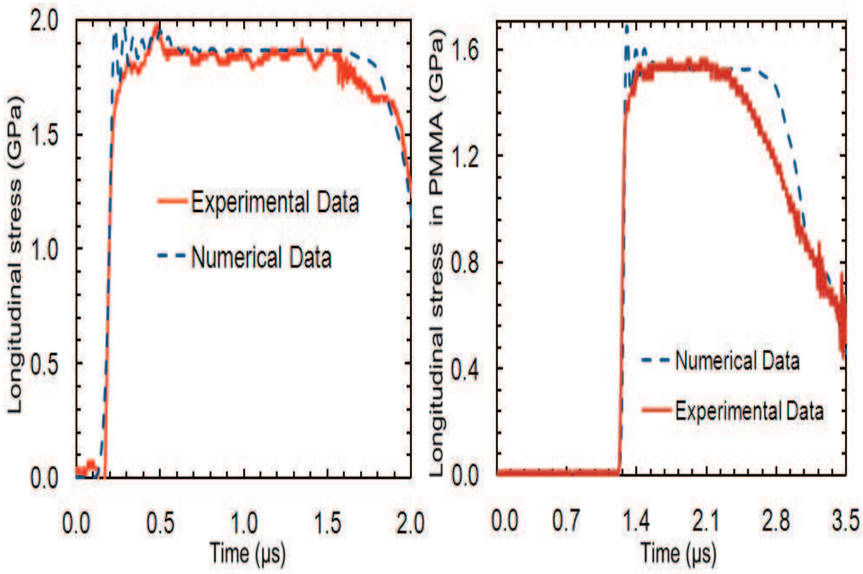

Fig. 2.2. Representative experimental gauge traces from the through thickness orientation at the 0 mm position and at the back surface respectively (see Millett et al. [21]). The specimen was 3, 8 mm thick. The impact conditions were a 5 mm dural flyer at $V = 504\ m/s$. The dotted curve is the numerical data obtained using proposed model Eqs. (1.1)–(1.10), the solid curve is the experimental data

(numerical simulation) and 2, 41 μs (experimental data) at the PMMA (see Fig. 2.2). The errors with respect to the experimental values are approximately 2, 6% (at the front surface) and 2.1% (at the PMMA), respectively. The Hugoniot Stress Levels (HELs) $\sigma_{HSL} = 1,87\ GPa$ (front gauge - Fig. 2.1) and $\sigma_{HSL} = 1,52\ GPa$ (rear gauge - Fig. 2.1) agree well with the experimental data. The loading and release traces are in good agreement with the experiment for both at the front surface and at the PMMA (see Fig. 2.1). Furthermore, maximum difference between the experimental data and new proposed model for the plateau stress was 6 %. The simulation based on proposed anisotropic EOS correctly predicts also separation of the flyer plate from the cover plate. In addition, this numerical simulation results using new material model show that the relationship between shock velocity and particle velocity through the thickness orientation can be also linearly approximated (Fig. 2.3), yielding the relation: $U_S^L = C_0^L + S_1^L u_p$, where $C_0^L = 3230 m/s$, $S_1^L = 0.98$.

Besides, another important characteristic, the arrival time to the HSL at the 0 mm position and back surface are in good correlation with experimental data. Further comparison shows that the pulse width and the reloading trace are in good agreement with the experimental data (see Fig. 2.2). The measurements (experimental and numerical) of the shock velocity through the thickness orientation with particle velocity show a linear response, similar to many other materials. No effects of specimen thickness have been noted during the numerical simulations for the range of thicknesses between 2,3 and 5,7 mm.

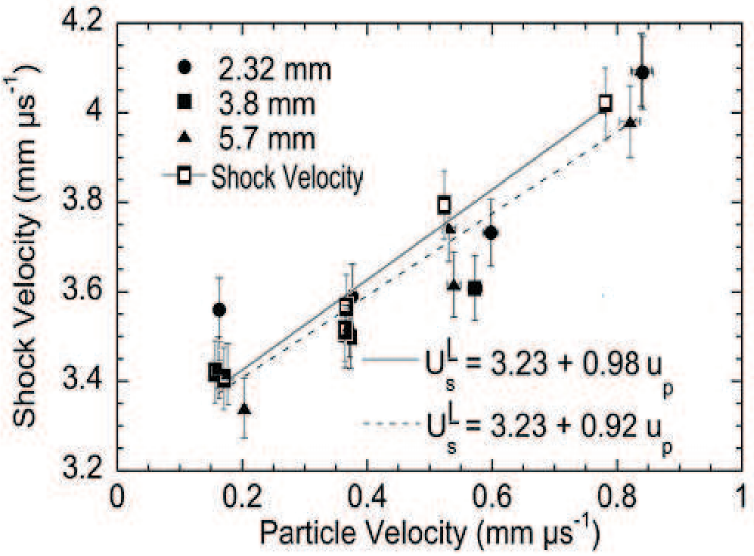

Fig. 2.3. Experimental data $U_S^L - u_p$ for the Carbon-Fibre-Composite material, showing the variation with specimen thickness (experimental data obtained by Millett et al. [21]). The dotted curve is calculated using experimental data for $U_S^L - u_p$, the solid curve is calculated using numerical simulation based on the material model Eqs. (1.1)–(1.10)

The good agreement between the results can be observed and leads to the conclusion that constitutive equation presented in this paper can be used for the simulation of shock wave propagation within CFC material. Reduction of the model to the conventional constitutive equations in the limit of isotropy allows for its use in modelling wide range of materials.

The main conclusion obtained from these results is that the equation of state (EOS), as it stands, is suitable for simulating shock wave propagation in anisotropic composite materials (CFC). However, further work is required both in the experimental and constitutive modelling areas to find a full description of anisotropic material behavior.

Conclusions

In this paper, thermodynamically and mathematically consistent constitutive equations suitable for characterizing shock wave propagation in an anisotropic composite (CFC) material are presented. An accurate extrapolation of high-pressure shock Hugoniot states to other thermodynamics states for shocked Carbon Fibre Composite (CFC) materials was presented. The proposed anisotropic equation of state represents mathematical and physical generalization of the Mie-Grüneisen equation of state for isotropic materials and reduces to this equation in the limit of isotropy. A generalised decomposition for separation of material volumetric compression (compressibility effects – EOS) from deviatoric strain effects is formulated, which allows for the consistent calculation of stresses in the elastic regime as well as in the presence of shock waves. According to this decomposition the pressure is defined as the state of stress that results in only volumetric deformation, and consequently is a diagonal second order tensor. Based on the generalised decomposition of stress tensor, the modified Mie-Grüneisen equation of state, and generalised Hook's law, a system of constitutive equations suitable for shock wave propagation have been formulated. In this paper, the behavior of the CFC material under shock loading conditions was also investigated. Plate impact experiments on CFC material were carried out by Millett et al. [21]. A comparison of the experimentally obtained general pulse shape and Hugoniot stress level with numerical simulation shows an excellent agreement and suggests that the EOS is performing satisfactorily. Furthermore, measurements (experimental and numerical) of the shock velocity through the thickness orientation with particle velocity show a linear response, similar to many other materials. No effects of specimen thickness have been noted during the numerical simulations for the range of thicknesses between 2,3 and 5,7 *mm*. However, further development of the constitutive equations taking into account strain rate sensitivity is required. This will require further work both on the experimental and constitutive modelling levels.

References

[1] Barker L.M., Hollenbach R.E. Laser interferometer for measuring high velocities of any reflecting surface // J. Appl. Phys. 1972. № 43(11). P. 4669–4675.

[2] Kanel G.I. Some new data on deformation and fracture of solids under shock-wave loading // J. Mech. Phys. Solids. 1998. № 46(10). P. 1869–1886.

[3] Possible applications of the ion beams technique for investigations in the field of equation of state / G.I. Kanel [et al.] // Nucl. Instr. and Meth. in Phys. Res. A. 1998. № 415(3). P. 509–516.

[4] Bourne N.K., Stevens G.S. A gas gun for plane and shear loading of inert and explosive targets // Rev. Sci. Instrum. 2001. № 72(4). P. 2214–2218.

[5] Bourne N.K. A 50 mm bore gas gun for dynamic loading of materials and structures // Meas. Sci. & Technol. 2003. № 14. P. 273–278.

[6] Davison L., Graham R.A. Shock Compression of solids // Phys. Rep. 1979. № 55. P. 255–379.

[7] Intense dynamic Loading of Condensed Matter / A.V. Bushman [et al.]. Washington: D.C. Taylor and Francis, 1993; Russ. original (OIKhF, Chernogolovka), 1988. 297 p.

[8] Meyers M.A. Dynamic Behavior of Materials. New York: Wiley. Inc., 1994. 668 p.

[9] Steinberg D.J. Equation of State and Strength Properties of Selected Materials // Report No. UCRL-MA-106439. Lawrence Livermore National Laboratory. Livermore: CA, 1991.
[10] Shock response of a glass–fiber-reinforced polymer composite / D.P. Dandekar [et al.] // Compos. Struct. 2003. № 61. P. 51–59.
[11] Munson D.E., May R.P. Dynamically determined high-pressure compressibilities of three epoxy resin systems // J. Appl. Phys. 1972. № 43(3). P. 962–971.
[12] The behaviour of an epoxy resin under one-dimensional shock loading / J.C.F. Millett [et al.] // J. Appl. Phys. 2002. № 92(11). P. 6590–6594.
[13] Glass-epoxy composite behaviour under shock loading / A.Z. Zhuk [et al.] // J. Phys. IV. 1994. № 4. P. 403–407.
[14] Equation of state properties of modern composite materials: modelling shock, release and spallation / W. Riedel [et al.] // Shock compression of condensed matter — 2003. Melville: N.Y.: American Institute of Physics, 2004. P. 701–704.
[15] Zaretsky E., de Botton G., Perl M. The response of a glass fibers reinforced epoxy composite to an impact loading // Int. J. Solids Struct. 2004. № 41. P. 569–584.
[16] Computer simulation of the heterogeneous materials response to the impact loading / G.I. Kanel [et al.] // Int. J. Impact Engineering. 1995. № 17. P. 455–464.
[17] High-velocity Impact of Graphite/Epoxy Composite Laminates / J.K. Chen [et al.] // Comp. Sci. and Techn. 1997. № 57. P. 1268–1379.
[18] Development of material models for Nextel and Kevlar-epoxy for high pressures and strain rates / C.J. Hayhurst [et al.] // Int. J. Impact Engineering. 1999. № 23(1). P. 365–376.
[19] Shock response of a unidirectional composite at various orientations of fibers / S.A. Bordzilovsky [et al.] // Shock compression of condensed matter-1997. Melville, NY: AIP Press, 1998. P. 545–548.
[20] Shock behaviour of 3D carbon–carbon composite / P.-L. Hereil [et al.] // J. Phys. IV. 1997. № 7. P. 529–534.
[21] The effect of orientation on the shock response of a carbon fibre-epoxy composite / J.C.F. Millett [et al.] // Composites Science and Technology. 2007. № 67(15-16). P. 3253–3260.
[22] Kiselev A.B., Lukyanov A.B. Mathematical Modeling of Dynamic Processes of Irreversible Deforming, Micro- and Macrofracture of Solids and Structures. // Int. J. Forming Processes. 2002. № 5. P. 359–362.
[23] A constitutive formulation for anisotropic materials suitable for wave propagation computer program-II / C.E. Anderson [et al.] // Comput. Mech. 1994. № 15. P. 201–223.

[24] Lukyanov A.A. Thermodynamically consistent anisotropic plasticity model // ASME Proceeding IPC 2006. ASME, 2006.
[25] Lukyanov A.A. Constitutive behaviour of anisotropic materials under shock loading // Int. J. Plasticity. 2008. № 24(1). P. 140–167.
[26] Lukyanov A.A. An equation of state for anisotropic materials under shock loading // Eur. J. Physics B: Condesed Matter and Complex System. 2008. № 64(2). P. 159–164.
[27] Lukyanov A.A. Thermodynamically Consistent Anisotropic Plasticity Model // J. Pressure Vessel Technology. 2008. 021701. № 130.
[28] Lukyanov A.A., Pen'kov V.B. State equation for anisotropic materials under shock loading // Vestn. Samar. Gos. Univ. Estestvennonauchn. Ser. 2008. № 2(61). P. 173–182.
[29] Lukyanov A.A., Pen'kov V.B. A mathematically correct model of incompressible anisotropic associated plasticity // Vestn. Samar. Gos. Univ. Estestvennonauchn. Ser. 2007. № 4(54). P. 280–289.
[30] Wallace D.C. Thermodynamics of Crystals. Mineola: Dover Publications Inc., 2003. 512 p.
[31] Johnson J.N., Shock Propagation Produced by Planar Impact in Linearly // J. Appl. Phys. 1971. № 42(13). P. 5522–5530.
[32] Johnson J.N., Calculation of Plane-Wave Propagation in Anisotropic Elastic-Plastic Solids // J. Appl. Phys. 1972. № 43(5). P. 2074–2082.
[33] Winey J.M., Gupta Y.M., Nonlinear anisotropic description for shocked single crystals: Thermoelastic response and pure mode wave propagation // J. Appl. Phys. 2004. № 96(4). P. 1993–1999.
[34] Hallquist J.O. LS-DYNA Theoretical Manual. Livermore: Livermore Software Technology Corporation, 1998. 498 p.

Paper received 4/*XII*/2009;
Paper accepted 4/*XII*/2009.

МОДЕЛИРОВАНИЕ УДАРНЫХ ВОЛН В КОМПОЗИЦИОННЫХ МАТЕРИАЛАХ

 А.А. Лукьянов[2]

Предложена аналитическая связь состояний Гюгонио с другими термодинамическими состояниями при высоких давлениях для углеродно-волокнистых композитов. Рассмотренное анизотропное уравнение состояния обобщает нелинейное уравнения Грюнайзера для изотропных материалов и редуцируется к классическому варианту в случае изотропии. Используя соотношения нелинейной анизотропной среды и обобщенную декомпозицию тензора напряжений, исследовано распространение ударных волн в углеродно-волокнистых композитах. Численные расчеты уровней напряжений Гюгонио хорошо согласуются с экспериментальными данными для выбранного углеродно-волокнистого композита. Результаты расчетов представлены и проанализированы, и будущие исследования намечены.

Ключевые слова: композит, конструкции, ударные волны, моделирование, декомпозиция тензора напряжений, уравнение состояния, удар.

Поступила в редакцию 4/*XII*/2009.
в окончательном варианте 4/*XII*/2009.

[2]Лукьянов Александр Алексеевич (aaluk@mail.ru), кафедра вычислительных машин Липецкого филиала Международного института компьютерных технологий, 398059, Россия, г. Липецк, пр. С. Кувшинова, 5Б.